Macromolecules
ARTICLE

*Macromolecules* **2010**, *43*, 671–679 **671**
DOI: 10.1021/ma902188c

# Cold Crystallization of Poly(trimethylene terephthalate) As Revealed by Simultaneous WAXS, SAXS, and Dielectric Spectroscopy

**Alejandro Sanz,* Aurora Nogales, and Tiberio A. Ezquerra**

*Instituto de Estructura de la Materia, CSIC, C/Serrano 121, Madrid 28006, Spain*

**Michelina Soccio, Andrea Munari, and Nadia Lotti**

*Dipartamento di Chimica Applicata e Scienze dei Materiali, Universitá di Bologna, Via Terracini 28, 40131 Bologna, Italy*

*Received October 5, 2009; Revised Manuscript Received November 3, 2009*

ABSTRACT: This work presents an experimental study on the interplay between structure and dynamics during isothermal and nonisothermal cold crystallization of poly(trimethylene terephthalate). Simultaneous X-ray scattering and dielectric spectroscopy measurements revealed that, during cold crystallization, crystalline lamellae tend to be homogeneously distributed along the sample. A significant amount of rigid amorphous phase is formed during cold crystallization, and its location is assigned to the crystal−amorphous interface. The formation of the rigid amorphous phase during cold crystallization is less effective for poly(trimethylene terephthalate) than for other similar aromatic polyesters like poly(ethylene terephthalate). The mobile amorphous phase, giving rise to the dielectric α relaxation, is mainly located between consecutive crystalline lamellae. The segmental dynamics of the amorphous phase is restricted by the growing crystals during both primary and secondary crystallization.

## 1. Introduction

Poly(trimethylene terephthalate) (PTT) belongs to the aromatic polyesters family and due to its excellent physical and processing properties has attracted both scientific and industrial interest as a promising engineering thermoplastic material.[1−3] Several works related to the melt crystallization of PTT have been recently published.[2−9]

PTT crystallizes from the melt with spherulite morphology, very regular lamellar stacking, and at a faster rate as compared to PET due to the more flexible chain. The formation of a rigid amorphous phase (RAP) during the crystallization of PTT has also been reported.[9−11] It was suggested to be located in the interface between the lamellar crystals and the amorphous regions.[7] The presence of RAP in PTT has been linked to the existence of cooperatively rearranging regions (CRR's) with sizes changing as a function of the crystallization conditions where a progressive restriction of cooperative motions of the remaining amorphous phase takes place.[4] However, less attention has been paid to the cold crystallization of PTT. Cold crystallization takes place at temperatures $T_c$ close to the glass transition temperature $T_g$ under deep undercooling ($T_m - T_c$) conditions, typically in totally amorphous samples obtained by deep quenching below the $T_g$. Under these circumstances, crystallization is kinetically driven because diffusion effects become dominant over thermodynamic conditions.[12] The existence of RAP has been also confirmed in PTT cold crystallized by DSC and dynamic mechanical analysis measurements.[13] Moreover, cold crystallization of PTT has been recently studied by an innovative method which takes advantage of the specific fluorescence emission of phenylene dimers from adjacent chains due to these interchain complexes can be just formed in the disordered state.[14] The latter study supports the existence of an induction period prior to the nucleation and growth where a densification of the polymeric chains occurs. In polymers, it is well-known the influence of the crystalline lamella on the segmental dynamics of the remaining amorphous region. In general, above the $T_g$, the segmental relaxation (α process), for instance as explored by means of dielectric spectroscopy (DS), is affected by crystals. This effect results in a less intense, broader, and slower relaxation curve.[15−21] Monitoring these changes during the crystallization phenomena, one can extract both dynamic and structural information on the amorphous fraction, which is certainly impossible just by using scattering or microscopy tools. By following the α relaxation dynamics by DS, the coexistence of two amorphous fractions in several semicrystalline polymers has been proposed.[18,22−25] DS measurements have corroborated the existence of a RAP, defined, at a given temperature, as an immobile amorphous region which is not able to relax at the same rate as the mobile amorphous fraction. The existence of RAP, postulated a long time ago,[26,27] seems to be a rather general feature for semicrystalline aromatic polymers like poly(ethylene terephthalate) (PET),[18,28] poly(butylene terephthalate) (PBT),[26,29] poly(butylene isophthalate) (PBI),[22] bisphenol A polycarbonate (BAPC),[30] poly(styrene) (PS),[31] and poly(ether ether ketone) (PEEK).[25,27,32,33] However, there is still no direct evidence about the location of such a RAP and whether this is a universal feature or depends on the nanostructure induced during crystallization. All these experimental showed above support the assumption of a three-phase model consisting of crystalline, amorphous, and rigid amorphous domains. It is well established that the physical properties of polymers are directly related to the structure, the morphology, and the dynamic behavior of the material. Therefore, a deep understanding of these features and their interrelationships is necessary from both fundamental and applied points of view.

*To whom correspondence should be addressed. E-mail: asanz@iem.cfmac.csic.es.



Published on Web 11/19/2009

In order to provide new information on this topic, this work presents experimental results on the isothermal and nonisothermal cold crystallization of PTT, studied by simultaneous measurements of wide- and small-angle X-ray scattering (WAXS and SAXS) and dielectric spectroscopy (DS). The main goal of the present work is to shed light on the structure−dynamics relationships during the cold crystallization of PTT.

## 2. Experimental Part

**2.1. Samples and Techniques.** Poly(trimethylene terephthalate) (PTT) was synthesized by the two-stage polycondensation method as described elsewhere.[34] The chemical structure was confirmed by means of $^1$H NMR, and the weight-average molecular weight, $M_w$, determined by GPC, turned out to be about 56 000. At room temperature the polymer appeared as a semicrystalline solid. Differential scanning calorimetry (DSC) measurements of the PTT sample were performed in order to evaluate the glass transition temperature ($T_g$) and the melting point ($T_m$). The values of $T_g$ and $T_m$ are 45.5 ± 1.5 °C and 227 ± 1 °C, respectively.[35] After drying the sample for 1 day under vacuum at a temperature of 100 °C, the powder was mold-pressed 5 °C above the $T_m$ and subsequently quenched into iced water. In this way, amorphous 0.2 mm films were obtained. Cold crystallization was investigated by simultaneous measurements of SAXS, WAXS, and DS. The combination of these techniques will be referred here after as SWD. The experiments were performed at the BM16 beamline of the European Synchrotron Radiation Facility (ESRF), Grenoble, France. The experimental setup at BM16 allows the simultaneous acquisition of two-dimensional (2-D) SAXS and WAXS images using CCD cameras. A complete description of the BM16 setup can be found elsewhere.[36] In order to carry out the SWD measurements, the dielectric spectrometer was installed at the BM16 beamline as done in previous experiments.[22,37] The dielectric equipment is based on a Novocontrol system integrating a SR830 lock-in amplifier with a dielectric interface. The simultaneous X-ray scattering processes and the application of the electric field to get the dielectric information are possible by using a homemade special sample holder. The characteristics of the SWD cell have been extensively described in a previous publication.[38] A circular piece of film with a diameter of 3 cm was sandwiched between the electrodes of the sample holder in order to perform the simultaneous measurements. Dielectric spectroscopy measures the complex dielectric constant $\varepsilon^*(\omega) = \varepsilon'(\omega) - i\varepsilon''(\omega)$ as a function of the applied frequency $\omega$. When the material undergoes a relaxation process where a dipole moment is involved, the imaginary part of the dielectric permittivity, $\varepsilon''(\omega)$, referred to as the dielectric loss, shows a maximum. The position in frequency of this peak provides information about the relaxation time associated with the underlying microscopic motion, which makes DS an extremely powerful tool for the dynamic characterization of polymeric materials among others.[15] The wavelength used in the X-ray scattering measurements was 0.1 nm. A $q$-range, where $q = 4\pi/\lambda \sin\theta$ is the scattering vector, $2\theta$ being the scattering angle, of 0.06−1.28 nm$^{-1}$ for SAXS and of 9.9−20 nm$^{-1}$ for WAXS was covered by appropriate positioning of the detectors.[36]

**2.2. Data Analysis.** WAXS patterns were analyzed in order to estimate the degree of crystallinity, $X_c$, of the sample as a function of either temperature or time. We consider the total scattering pattern as a linear combination of the crystalline ($X_{crystal}$) and amorphous contributions ($X_{amorphous}$) as follows:

$$I(q,t) = X_{crystal}(t)I_{crystal}(q) + |1 - X_{crystal}(t)|I_{amorphous}(q) \quad (1)$$

where $X_{crystal}$ is the fraction of crystalline material, $I_{crystal}$ is the intensity from the Bragg peaks, and $I_{amorphous}$ is the intensity from the amorphous halo.

Therefore, the crystalline amount can be estimated from the ratio between the area below the crystalline peaks, $A_c$, to the total scattered area, $A_c + A_a$, by

$$X_c = \frac{A_c}{A_c + A_a} \quad (2)$$

The contribution of the amorphous halo was taken from the initial pattern (crystallization time $t_c = 0$ or initial temperature for the nonisothermal crystallization $T = 47$ °C). The average distance between the crystalline lamella and the amorphous domains is obtained from the maximum shown by the SAXS profiles after subtraction of the background using the following equation:

$$L = \frac{2\pi}{q_{max}} \quad (3)$$

The scattering invariant was calculated from the SAXS measurements as

$$Q = \int_{q_{min}}^{q_{max}} Iq^2 \, dq \quad (4)$$

Dielectric loss data were analyzed in terms of the Havriliak−Negami formalism.[15,39] This empirical equation describes the imaginary part of the dielectric constant as follows:

$$\varepsilon'' = \left(\frac{\sigma}{\varepsilon_0 \omega}\right)^s + \mathrm{Im}\left(\frac{\Delta\varepsilon}{[1+(i\omega\tau_{HN})^b]^c}\right) \quad (5)$$

where $\sigma$ is the direct current electrical conductivity, $\varepsilon_0$ is the vacuum permittivity, the coefficient $0 < s < 1$ depends on the conduction mechanism, $\omega$ is the angular frequency ($\omega = 2\pi F$, $F$ being the frequency), $\Delta\varepsilon$ is the dielectric strength of the relaxation, $\tau_{HN}$ is the most probable value of the relaxation time distribution function, and $b$ and $c$ are shape parameters related to the symmetric and asymmetric broadening, respectively. Finally, the average relaxation $\tau$ time was calculated using the equation

$$\tau = \frac{1}{2\pi F_{max}} = \tau_{HN}\left[\sin\frac{b\pi}{2+2c}\right]^{-1/b}\left[\sin\frac{bc\pi}{2+2c}\right]^{1/b} \quad (6)$$

## 3. Results

**3.1. Nonisothermal Crystallization by Simultaneous SAXS, WAXS, and DS.** Figure 1 collects structural and dynamic information on the nonisothermal cold crystallization of PTT obtained by simultaneous measurements of WAXS, SAXS, and DS during a heating ramp of ≈0.8 °C/min above $T_g$. The evolution of WAXS patterns with temperature is displayed in Figure 1. The first two frames show a broad maximum, typically of amorphous materials confirming the initial amorphous nature of the sample. As temperature increases, Bragg peaks develop as a consequence of the crystallization process. In a parallel way to the Bragg peaks appearance, an increase of the scattered intensity at low angles in the SAXS patterns (Figure 1) is observed at $T \approx 57$ °C. This excess of SAXS intensity develops into a well-defined maximum due to the presence of a periodicity between crystalline lamella and disordered domains. Figure 1 also shows the evolution of the imaginary part of the dielectric constant during the nonisothermal crystallization of PTT (DS). The initial dielectric spectrum shows the typical α relaxation associated with the segmental motions of the

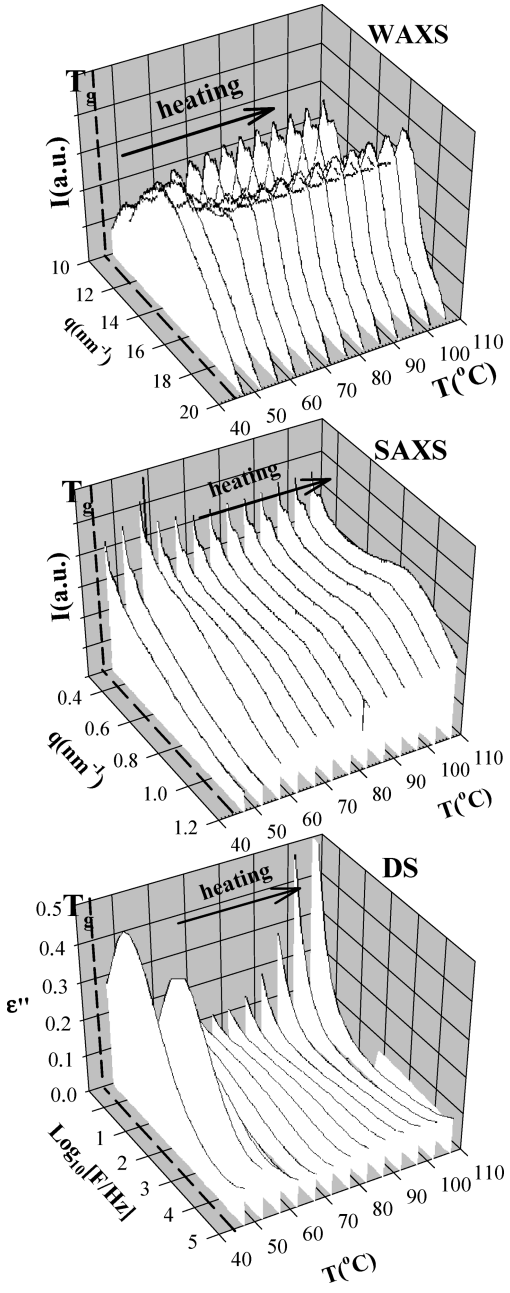


**Figure 1.** Nonisothermal crystallization of initially amorphous PTT followed by WAXS (top), SAXS (center), and DS (bottom), at selected temperatures. WAXS and SAXS intensities are represented as a function of scattering vector $q$. The bottom panel shows the evolution of the dielectric loss $\varepsilon''$ with frequency.

amorphous chains above the $T_g$. As expected, the position of the peak shifts to higher frequencies with temperature. Around 62 °C, a dramatic reduction of the intensity of the relaxation curve takes place coinciding with the development of the Bragg peaks. At this temperature, the area underneath the relaxation curve decreases. This effect can be directly related to a progressive reduction of the dielectric strength, $\Delta\varepsilon$, during the crystallization of the polymer. Additionally, the onset of the crystallization also induces a sudden shift of the relaxation curve to lower frequencies. At higher temperatures, the maximum of the relaxation curve continues moving toward higher frequencies, following the normal behavior when temperature increases. Even at higher temperatures, an increase of intensity in $\varepsilon''$ in the low-frequency side is observed corresponding to the contribution of the electrical conductivity. As an example, some frames at selected temperatures are shown in Figure 2 for the SWD experiment. The continuous lines in Figure 2 for the left (DS) and central (WAXS) panels represent the fits of the experimental data to eqs 5 and 1, respectively. By means of the data analysis described previously, it was possible to correlate structural magnitudes (crystallinity $X_c$ and long period $L$) with dynamic parameters extracted from the dielectric measurements. As shown in Figure 3a, $X_c$ increases gradually with temperature, reaching almost a 30% at 107 °C. The sigmoidal shape in the dependence of $X_c$ with temperature suggests that 30% is approximately the maximum value of crystallinity achievable for PTT by means of dynamic cold crystallization. Figure 3b displays the variation of the long spacing during the nonisothermal cold crystallization of PTT. The values of long spacing first decrease during the initial stages and later remain almost constant between 80 and 110 °C with an approximate value of 7 nm. Figure 3c displays the evolution of the scattered invariant at low angles with temperature. The apparent SAXS invariant suffers a discontinuous increase with temperature during the entire $T$ range. From the fitting of the empirical Havriliak−Negami function (eq 5) to the experimental dielectric spectrum, it is possible to estimate the $\Delta\varepsilon$, the average relaxation time and the shape parameters of the α relaxation process. In Figure 2 (left) the dotted lines indicate the different contributions to the dielectric spectrum according to eq 5. At high frequencies, the low-frequency tail of the $\beta$ relaxation has been considered according to standard procedures.[18,22,40] Figure 4 shows the dielectric magnitudes for the dielectric α process of PTT as a function of temperature during the heating process. The dielectric strength exhibits a continuous decrease with temperature (Figure 4a), especially dramatic around 60 °C where the onset of the crystallization process is located. It is well-known that the magnitude of the dielectric strength $\Delta\varepsilon$ can be related, in a first approach, to the fraction of mobile dipoles or, in other words, to the fraction of mobile disordered material.[15,41] Figure 4b displays the evolution of the α relaxation time with temperature. Below 60 °C, the relaxation time becomes faster as temperature increases as expected for the α relaxation of any glass former. For the three points below 60 °C, the temperature evolution of the α relaxation time shows the expected non-Arrhenius behavior for cooperative motions. In general, the curvature showed by the α relaxation can be described by the Vogel−Fulcher−Tamman equation.[15] However, this kind of analysis is beyond the scope of this work. On the other hand, around 60 °C, the α relaxation time $\tau$ exhibits a sharp discontinuity. At higher temperatures, the values of $\tau$ continue to get faster as temperature increases. Figure 4c shows the variation of the HN parameters, which define the shape of the relaxation curve with temperature. On one hand, the parameter $b$, related to the symmetrical broadening of the curve, decreases with temperature, indicating that the relaxation time distribution becomes broader. On the other hand, the parameter $c$ increases, and it becomes nearly 1 for 57 °C. The overall complex behavior with temperature displayed in Figures 3 and 4 is obviously a consequence of the nonisothermal crystallization process of PTT during heating above the $T_g$. All these findings will be discussed extensively in the Discussion section.

**3.2. Isothermal Crystallization by Simultaneous SAXS, WAXS, and DS.** In Figure 5, we represent the results obtained by using SWD to monitor the isothermal crystallization of PTT at 52 °C. At this temperature, the α relaxation is well located inside the accessible frequency window, and the time required to complete the frequency sweep

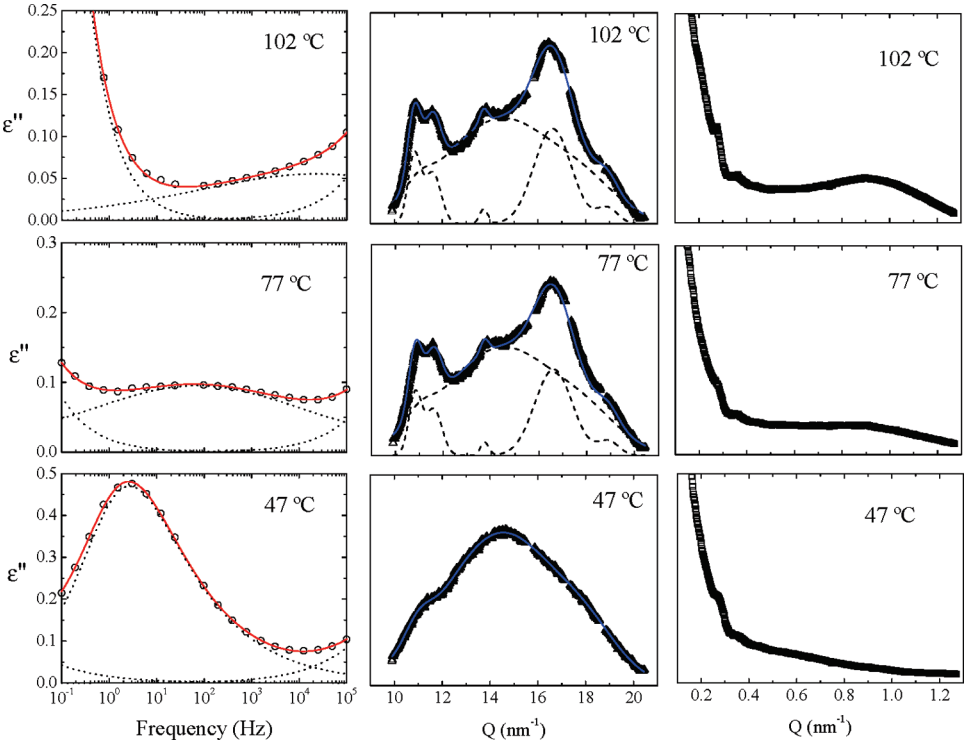


**Figure 2.** Selected snapshots during nonisothermal crystallization of PTT. Dielectric spectra (left panels) data are fitted to the HN equation. Dotted lines indicate separate contributions from α relaxation, high-frequency tail of the $\beta$ process and low-frequency contribution of the electrical conductivity. Experimental WAXS patterns (central panels) are described by a linear combination of crystalline (Gaussian peaks) and amorphous contributions (amorphous halo). Right panels collect the experimental SAXS profiles as a function of $q$ at selected temperatures.

(≈ 2 min) is appropriate to monitor a time-resolved experiment. On the left, the evolution of the dielectric loss as a function of frequency is displayed at different stages of the crystallization process. WAXS (central panels) and SAXS (right panels) patterns are shown for the same crystallization times. As expected, the α relaxation curve becomes broader and shifted to lower frequencies with the crystallization time. The growing of the crystalline lamellae is also manifested by the emerging of Bragg peaks in the WAXS profiles. The amorphous nature of the starting material is demonstrated by the absence of crystalline reflections at 0 min. It must be noted the lack of any excess of scattered intensity in the SAXS patterns for the isothermal crystallization at 52 °C. Again, by using eqs 1 and 2, in Figure 6 it is shown the evolution of crystallinity with time during different isothermal experiments. As expected, for the cold crystallization regime, the crystallization rate and final crystallinity increase with temperature. The final values of crystallinity range from 17 to 25% for crystallizations at 47 and 57 °C, respectively. No evidence of SAXS peaks below 52 °C was detected during the isothermal crystallization of PTT. The dielectric parameters obtained after fitting the eq 5 to the experimental relaxation curve are collected in Figure 7 as a function of the crystallization time. The contribution of the tail of the $\beta$ relaxation was taken into account.[18,22,40] The latter contributes to the high-frequency tail of the dielectric spectra. As one can see (Figure 5), the $\beta$ relaxation at the temperature of the experiment is well separated from the α relaxation and does not affect significantly its description in terms of the HN equation. As shown in Figure 7a, the dielectric strength values for the α relaxation decrease during the crystallization process. Respect to the shape parameters of the α relaxation, Figure 7b displays the decrease of the symmetric broadening, $b$, and the increase of the asymmetric broadening, $c$, respectively. In other words, the α relaxation curve becomes broader and more symmetric during crystallization. As shown in Figure 7c, the average relaxation time for the α process, calculated by eq 6, tends to be slower with crystallization time in a linear fashion with time during the entire crystallization period. For comparison and due to the simultaneous acquisition of WAXS and DS measurements, Figure 7d shows the dependence of crystallinity with time, exhibiting the expected sigmoidal trend. Therefore, we can correlate the dielectric parameters with crystallinity. This information is collected in Figure 8. The dielectric strength (Figure 8a) for the α process decreases with crystallinity following the same trend during the whole range. This result slightly differs with previous studies on related aromatic polyesters where the dependence of the $\Delta\varepsilon$ with crystallinity shows two different regimes.[22,42] On the contrary, the evolution of the shape parameters with the degree of crystallinity shows the expected trend as shown in Figure 8b, becoming the α relaxation curve more symmetric and broader. Figure 8c shows that the α relaxation time exhibits two regimes. First, there is an initial slowing down of the relaxation time with increasing crystallinity. Then, a stronger dependence is observed for $X_c > 15\%$. This indicates that the restriction of the α relaxation dynamics, induced by the growing crystalline lamella, seems to shows two scenarios depending on the amount of crystals filling the remaining amorphous material.

## 4. Discussion

**4.1. Structural and Dynamic Evolution during Nonisothermal Crystallization.** The main experimental features extracted from this study are the following. PTT can be cold crystallized upon heating, reaching a final degree of crystallinity of ≈30%. The appearance of a maximum in the SAXS profiles (Figure 1) confirms that PTT crystallizes into a distribution of lamellar crystals separated by amorphous

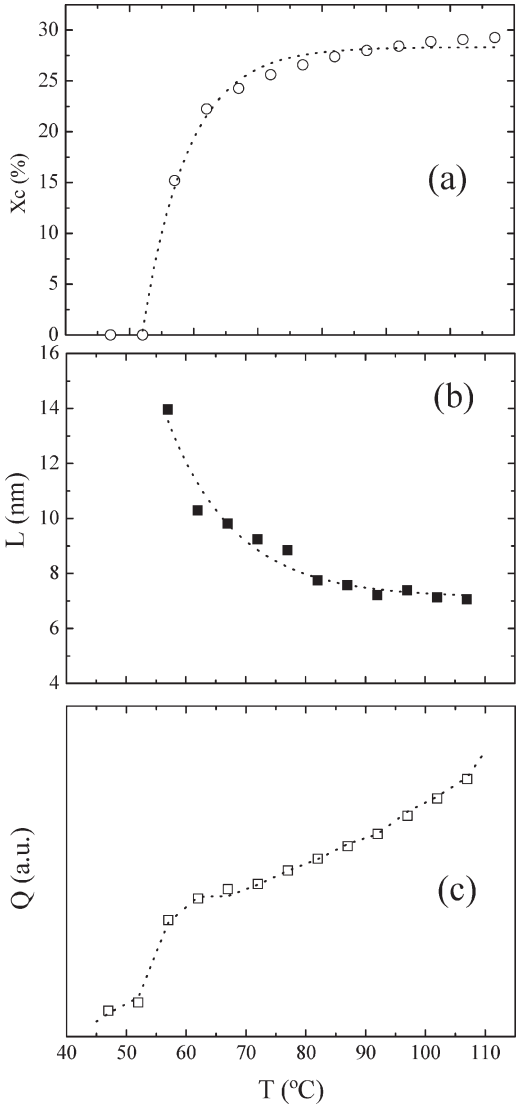


**Figure 3.** Dependence of the degree of crystallinity (a), long spacing $L$ (b), and apparent invariant (c) with temperature during nonisothermal cold crystallization of PTT. Dotted lines are guides to the eye.

regions. The evolution of the crystallinity with temperature (Figure 3a) exhibits the characteristic features of a primary regime, for $T < 60$ °C, and a secondary regime at higher temperatures. During the primary regime there is a concurrent increase of the invariant (Figure 3c) and a significant decrease of the long spacing (Figure 3b). This is consistent with the appearance of lamellar stacks filling in the sample volume. The initial decrease of the long spacing during primary crystallization is also a common finding for isothermal crystallization processes.[22,33,43] The observed initial decrease of $L$ (Figure 3b) can be connected with the sequential formation of either new crystal lamellae or lamellar stacks or both in the interlamellar amorphous regions.[44] At $T > 60$ °C, the dependence with temperature of both crystallinity and long spacing tends to be slower. However, the invariant exhibits a significant increment with temperature. This is consistent with a secondary crystallization regime in which new lamellae are forced to grow in the remaining interlamellar stacks amorphous regions.[45] We also find that the apparent SAXS invariant tends to increase more than the crystallinity for the late stages of the nonisothermal crystallization. Even though a quantitative comparison between $X_c$ and $Q$ must be carefully done, the strong increase of $Q$ with $T$

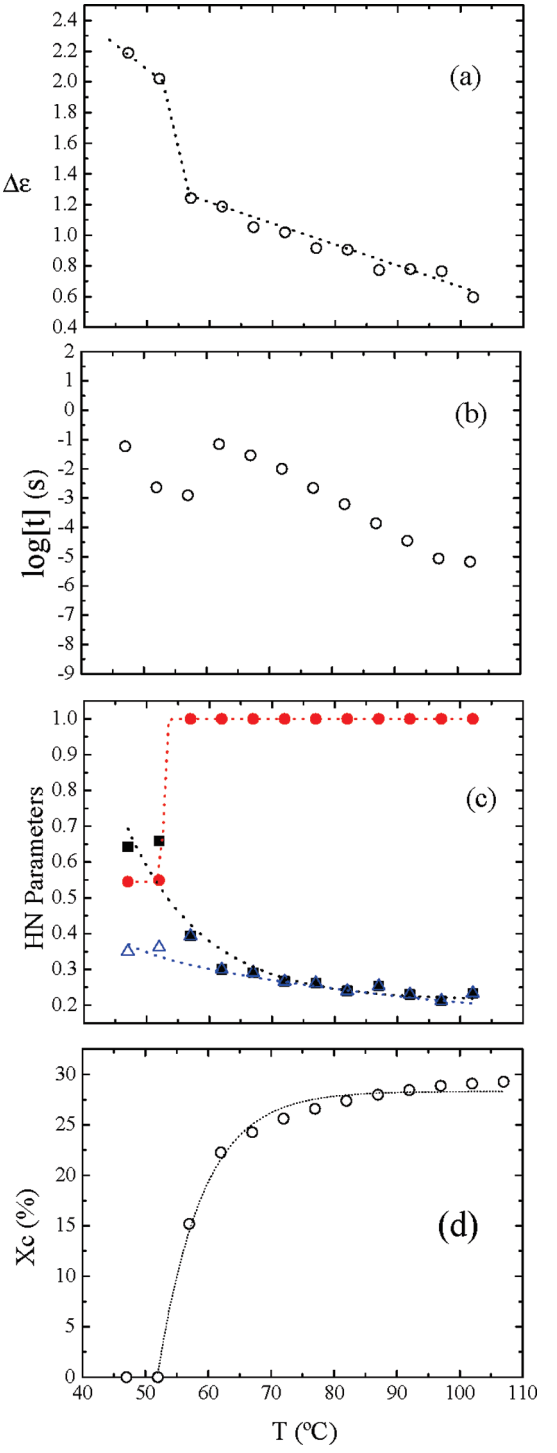


**Figure 4.** (a) Variation of the dielectric strength as a function of temperature during nonisothermal crystallization of PTT. Dotted line is a guide to the eye. (b) Evolution of the average relaxation time of the α mode. Continuous line represents the VFT fit for the relaxation time values of the totally amorphous material. (c) Evolution with temperature of the broadening parameters $b$ (■) and $c$ (●) of the HN empirical equation. It is also showed the product of $bc$ (△) during nonisothermal crystallization. (d) For comparison, evolution with $T$ of the degree of crystallinity obtained by simultaneous SWD measurements. Dotted lines are guides to the eye.

displayed by Figure 3c could be also induced by a larger difference between the electron densities of lamellar crystals and amorphous layers.[46] The final value of the long spacing $L$ estimated from the SAXS curves is around 6.5 nm, remaining almost constant during the whole temperature

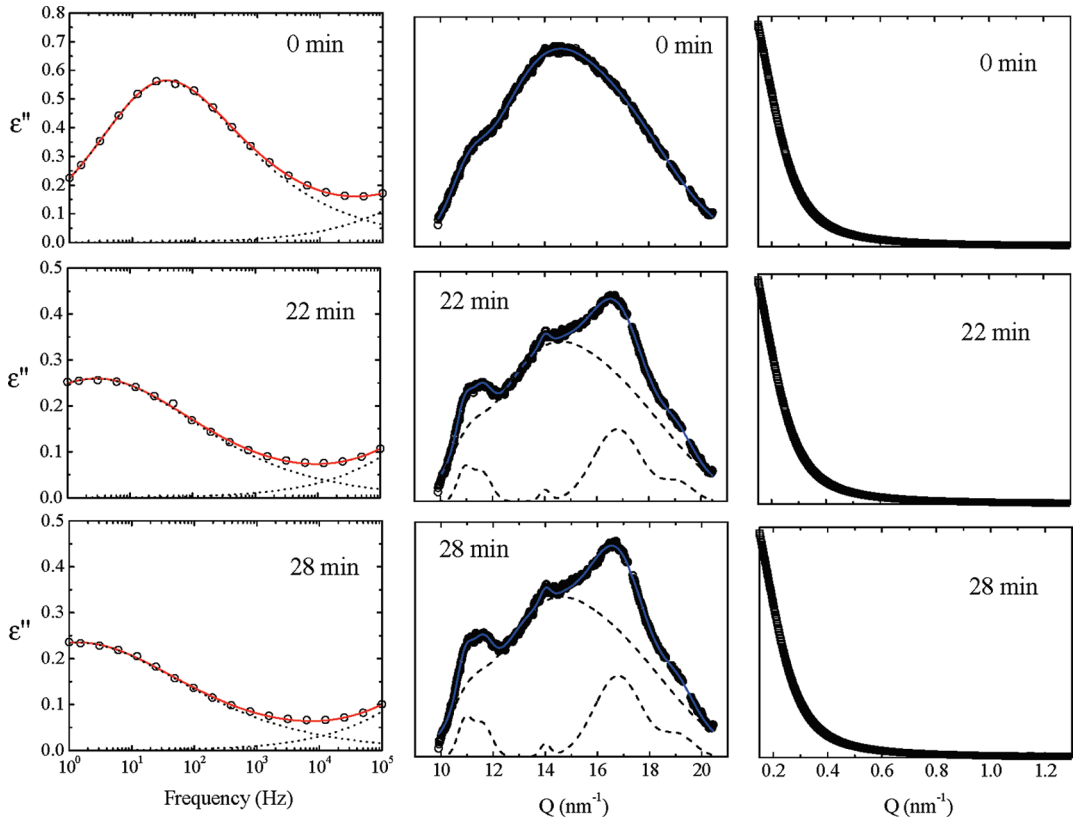


**Figure 5.** Time evolution of the dielectric relaxation curve (left), WAXS (center), and SAXS (right) patterns during isothermal cold crystallization of PTT at 52 °C. Experimental data are fitted to the same equations as described in Figure 2.

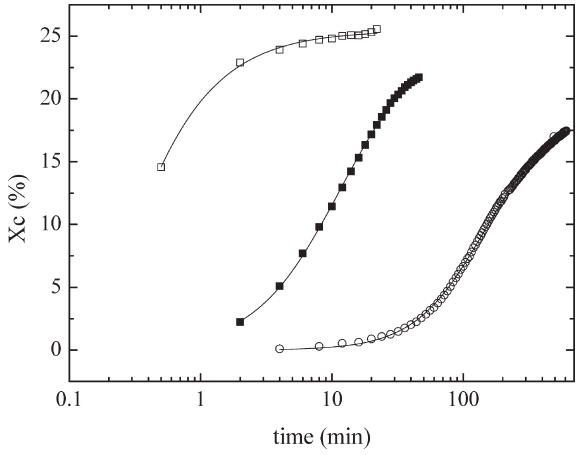


**Figure 6.** Crystallinity as a function of time for isothermal cold crystallizations at 47 (○), 52 (■), and 57 °C (□). Continuous lines are guides to the eye.

range. This value is lower compared to previous results obtained during isothermal melt crystallization of PTT where larger values of $L$ between 8 and 15 nm have been reported,[4,5] which is not surprising because of the influence of temperature on the polymeric morphology. The onset of the crystallization of PTT during heating above the $T_g$ can be also detected by simultaneous DS measurements. The area of the dielectric relaxation curves, known as dielectric strength $\Delta\varepsilon$, is related to the fraction of mobile dipoles involved in the relaxation process.[15] During crystallization, the polymeric chains incorporate into the growing crystals and cannot longer relax. The onset of crystallization is manifested by the dramatic decrease of $\Delta\varepsilon$ shown in Figure 4a. In general, the dielectric strength of an amorphous polymer decreases with temperature whereas for semicrystalline polymers slightly increases.[16,32] During heating, the increase of crystallinity with temperature is the main factor contributing to the decrease of $\Delta\varepsilon$. In general, the α relaxation time tends to increase during crystallization.[16−19,22,23,32] Upon heating, we observe a sudden increase of $\tau$ at the onset of crystallization (≈ 60 °C). Once the sample first crystallizes, $\tau$ follows the expected behavior decreasing as a function of temperature. Therefore, the progressively faster rate of the relaxation with temperature is dominant over the dynamic restriction imposed by the emerging crystals. But the presence of crystals affects not only the intensity of the dielectric relaxation curve but also its broadening and position. In more precise terms, the parameters $b$ and $c$ decrease and increase, respectively. In other words, the α relaxation curve becomes broader and more symmetric. Under the framework of the model proposed by Schlosser and Schönhals,[47,48] $b$ and the product $bc$ are related to large and small scale motions, respectively. As expected, the parameter $b$ of the α relaxation of PTT decreases (broader relaxation) with increasing crystallinity during heating above $T_g$. This can be interpreted as due to the higher hindrance to large scale motions imposed by the presence of crystals. However, as shown of Figure 4c, the product $bc$ does not vary as much as $b$ during crystallization. Generally, crystallization should not severely modify the $bc$ values due to its relation to small scale modes.[47,48] The slight decrease of $bc$ observed here could be related to the heterogeneity provoked by the interfaces between the crystalline and amorphous regions.[47,48] It should be noted that all these interpretations must be considered as approximations because $b$ and $c$ are also temperature-dependent parameters. The main driving force to perform simultaneous structural and dynamic experiments is to have access to

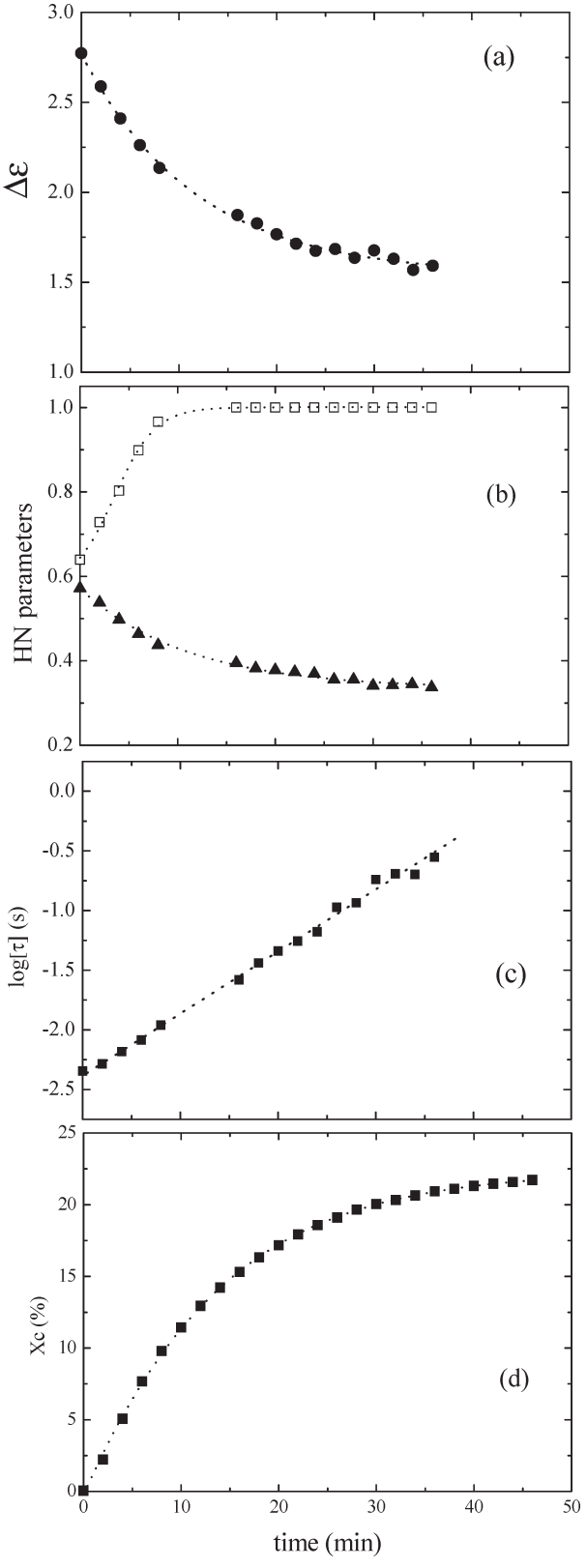


**Figure 7.** HN parameters obtained from the fitting of the dielectric spectra to the empirical HN equation for the crystallization of PTT at 52 °C. (a) Dielectric strength for the α relaxation. (b) Broadening parameters $b$ (▲) and $c$ (□) for the α relaxation. (c) Average relaxation time for the α process. All parameters are represented as a function of the crystallization time. (d) For the sake of comparison, evolution with time of the degree of crystallinity obtained by simultaneous SWD measurements. Dotted lines are guides to the eye.

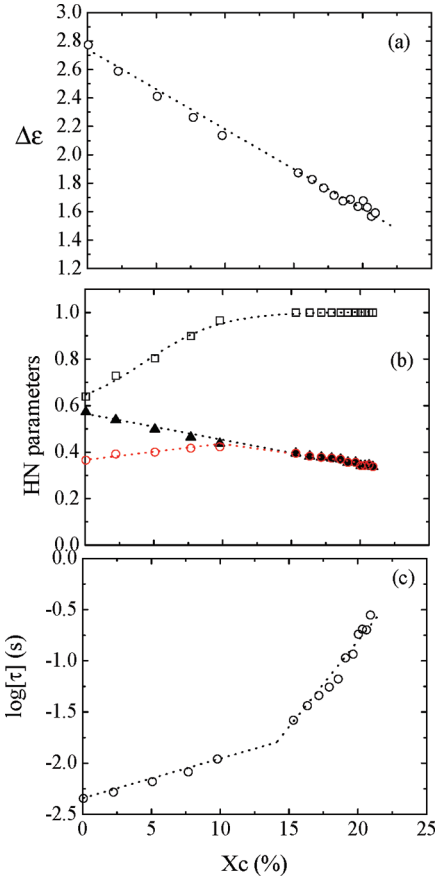


**Figure 8.** Dependence of HN parameters for the α relaxation with the degree of crystallinity estimated as by WAXS measurements for isothermal cold crystallization at 52 °C. (a) Dielectric strength. (b) Broadening parameters $b$ (▲) and $c$ (□) and product $bc$ (○). (c) Average relaxation time. Dotted lines are guides to the eye.

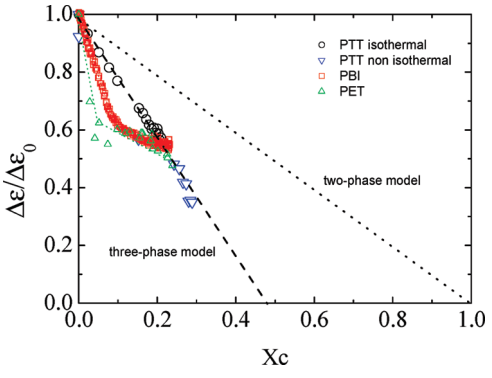


**Figure 9.** Normalized dielectric strength to its initial value for the α relaxation of PTT as a function of the crystallinity $X_c$ for isothermal cold crystallization at 52 °C (○) and nonisothermal crystallization (▽). Dotted line refers to an ideal two-phase model, and dashed line is a guide to the eye to illustrate how the data are closer to a three-phase model based on crystals, amorphous domains, and an interlamellar rigid amorphous phase. Data for PBI (□) and PET (△) isothermally cold crystallized at 60 and 96 °C, respectively, are included for comparison.[18,22] Dotted green line is a guide to the eye for the PET data.

information relating both the crystalline and the amorphous phases. In a first approach, the dielectric strength is related to the amount of mobile amorphous phase while crystallinity relates to the amount of material included in the crystals. Figure 9 shows the dependence of the dielectric strength, normalized to its initial value, as a function of the crystallinity for the dynamic cold crystallization (blue inverted

triangles). The dielectric strength decreases lineally with $X_c$. This fact supports the hypothesis that the rate of reduction of relaxing species is nearly constant during the crystallization process. As observed in Figure 9, the normalized $\Delta\varepsilon$ decreases with $X_c$ with a slope much steeper than $-1$. This can be interpreted as an indication that, during nonisothermal crystallization, the immobilized polymer segments are not only those included in the crystals. On the contrary, there should be a significant fraction of nonrelaxing and noncrystallized segments. We have previously mentioned that a common structural feature of polymers with a medium degree of crystallinity is the existence of a fraction of amorphous material which cannot relax at the same rate than the main disordered matrix. In general, the relaxation rate of this disordered fraction of material is slow enough to be considered as a rigid amorphous phase (RAP). As dynamic crystallization implies the formation of crystals at different temperatures without reaching the final equilibrium state, then an inherently more heterogeneous morphology is expected in this case as compared with that of isothermal crystallization. Therefore, in the next section we will discuss the isothermal SWD results, and a comparison with the nonisothermal ones will be established.

**4.2. Structural and Dynamic Evolution during Isothermal Crystallization.** Isothermal cold crystallization was also studied at different temperatures. The evolution of crystallinity with time shows the expected sigmoidal shape (Figure 6). In the particular case of PTT, this sigmoidal behavior has been reported for both melt and cold crystallization. The results presented here are in agreement with a recent work where the authors, by means of fluorescence emission spectroscopy measurements, propose that a four-step crystallization process takes place.[14] They suggest that, previous to the nucleation period, a densification of the material by parallel arrangement of the chains occurs. Subsequently, nucleation, growth, and secondary crystallization complete the ordering mechanism. As the reader can see from Figure 6, crystallization rate and final degree of crystallinity depend on the annealing temperature, as expected considering that cold crystallization of polymers is a temperature-activated process. The final degree of crystallinity slightly increases as a function of the crystallization temperature. It must be noted that the maximum in the SAXS profile due to the long-range periodicity of the crystalline lamellar stacks appears for $T_c >$ 60 °C. The absence of long spacing in the SAXS experiments or even any significant change in the SAXS patterns at $T <$ 60 °C may be an indication that the average distance among gravity centers of consecutive lamellae is larger than the maximum distance explored by us. Also, an excess of forward scattering from the SWD sample holder could mask the SAXS peak at low temperatures. In any case, this would be consistent with a rather homogeneous filling of the sample volume by single lamellae keeping relatively large distances among then. It is well established that near the $T_g$ polymer crystallization is kinetically controlled. Therefore, it is expected that by increasing the crystallization temperature, the diffusion of the polymeric chains to the growing crystals is facilitated, and hence, lamellae stacking can be favored, giving rise to the appearance of lamellar stacks showing long spacing in SAXS. The isothermal SWD experiment at 52 °C allowed us to precisely correlate dynamic information with structural one (Figures 8 and 9). Similarly as for the previous case of nonisothermal crystallization, the dielectric strength, Figure 9 (circles), decreases lineally with $X_c$ with the same slope for the whole range. This fact indicates that the rate of reduction of relaxing species is nearly constant during the crystallization process. Similar studies on analogous aromatic polyesters showed that the dependence of $\Delta\varepsilon_{nor}$ with $X_c$ changes the slope drastically from values lower than $-1$ to values close to $-1$.[20,22,42] As mentioned before, the formation of RAP during crystallization is a common feature for polymers with a medium degree of crystallinity. In general, close to $T_g$ the relaxation rate of the RAP is slow enough to be considered as rigid. Morphological studies on melt-crystallized PTT suggest a quite homogeneous crystal lamellae filling with absence of large amorphous pockets.[5] Considering that the amount of RAP can be related to the morphology developed during crystallization, it is expected that the crystallization for PTT differs from the one shown, for instance, by PET and PBI, where a heterogeneous distribution of the layered crystals (stacks of lamellae separated by liquid pockets) takes place.[18,22,42] For these polymers, it was proposed that the RAP is located in the interlamellar amorphous regions, being the material in the liquid pockets (interlamellar stacks amorphous regions) the main relaxing species giving rise to the dielectric α relaxation. These effect can be visualized in Figure 9 where we included $\Delta\varepsilon_{norm}$ data for PET[18] (triangles) and PBI[22] (squares). The dependence of $\Delta\varepsilon_{norm}$ with $X_c$ for PET and PBI significantly differs both qualitatively and quantitatively from that followed by PTT. First, PET and PBI exhibit initial strong decrease of $\Delta\varepsilon_{norm}$ with $X_c$ which was associated with the immobilization of the intralamellar stacks amorphous regions and second a weaker dependence associated with the formation, during secondary crystallization, of secondary lamellar stacks in the liquid pockets. For PTT, the reduction of $\Delta\varepsilon_{norm}$ with $X_c$ is weaker than in the previous cases and exhibits a single regime. This can be interpreted considering for PTT a homogeneous filling of the space by uniformly separated crystalline lamellae rendering to an absence of liquid pockets. In this case the RAP should be associated with the crystalline−amorphous interface rather than to the whole interlamellar amorphous regions. Polymers like PET and PBI with heterogeneous crystalline lamellar filling tend to form during primary crystallization higher amount of RAP than PTT. For this reason PTT exhibits a weaker reduction of $\Delta\varepsilon_{norm}$ with $X_c$.

A further support for this interpretation arises from the evolution with time (Figure 7c) and crystallinity (Figure 8c) of the α relaxation time. The logarithm of the α relaxation time increases linearly with time. In other words, the dynamics of the remaining amorphous phases is restricted by the emerging crystals over the whole crystallization process. This is a clear difference by comparison with previous information on PET and PBI where the onset of the slowing down of the segmental dynamics arises when secondary crystallization starts ($X_c \approx 15\%$). In the present case, PTT is dynamically restricted even during the primary crystallization. However, it must be noted that the dynamic restriction becomes more drastic when the degree of crystallization reaches values of around a 15%. As previously discussed, Figure 9 shows that the rate of formation of RAP is significantly lower for PTT than for other related aromatic polyesters. For semicrystalline PTT we propose that the fraction of amorphous materials giving rise to the α relaxation is located in the interlamellar domains. For stronger RAP forming polymers like PET and PBI, it was suggested[18,22] that the interlamellar amorphous regions were dynamically frozen during the primary crystallization being the liquid pockets, associated with the interlamellar stacks amorphous domains regions where the α relaxation originates. If for PTT one considers again a homogeneous filling of the space by uniformly separated crystalline lamellae and a RAP mainly situated in the crystal−amorphous interface, then it is expected the dynamic restriction imposed by the

crystalline lamellae to be effective already during primary crystallization. However, also for PTT, secondary crystallization, probably caused by the thickening of the existing lamellae, marks a drastic slowing down of the segmental dynamics (Figure 8c).

## 5. Conclusions

In summary, our results support the idea that for PTT the crystal lamellar stacks are homogeneously distributed, lacking of broad amorphous domains, liquid pockets, as observed for other similar polyesters. Consequently, the remaining amorphous phase which is able to relax giving rise to the dielectric α relaxation must be located between consecutive crystalline lamellae. Accordingly, the cold crystallization of PTT takes place by homogeneous filling of crystalline lamellar stacks. Our data suggest that the mobile amorphous phase is located in the interlamellar domains and the RAP is presumably located in the amorphous−crystal interface. The interlamellar amorphous regions are physically constrained by the surrounding crystals provoking a slowing down of the segmental dynamics during both primary and secondary crystallization.

**Acknowledgment.** This work has been funded by the Spanish CICYT (MAT2008-03232). A.S. also acknowledges the Higher Council for Scientific Research (CSIC) for the JAE-doc tenure. Financial support CICYT MAT2008-03232 is also acknowledged. The authors thank the ESRF for beam time and Francois Fauth and Ana Labrador for technical assistance during experiments at BM16.

## References and Notes

(1) Wu, J.; Schultz, J. M.; Samon, J. M.; Pangelinan, A. B.; Chuah, H. H. *Polymer* **2001**, *42*, 7141–7151.
(2) Yun, J. H.; Kuboyama, K.; Ougizawa, T. *Eur. Polym. J.* **2004**, *40*, 811–818.
(3) Grande, J. A. *Mod. Plast.* **1997**, *74*, 97–97.
(4) Hong, P. D.; Chuang, W. T.; Yeh, W. J.; Lin, T. L. *Polymer* **2002**, *43*, 6879–6886.
(5) Ivanov, D. A.; Bar, G.; Dosiere, M.; Koch, M. H. J. *Macromolecules* **2009**, *41*, 9224–9233.
(6) Huang, J.-M.; Chang, F.-C. *J. Polym. Sci., Part B: Polym. Phys.* **200**, *38*, 934–941.
(7) Kalakkunnath, S.; Kalika, D. S. *Polymer* **2006**, *47*, 7085–7094.
(8) Xue, M.-L.; Sheng, J.; Yu, Y.-L.; Chuah, H. H. *Eur. Polym. J.* **2004**, *40*, 811–818.
(9) Sisti, L.; Finelli, L.; Lotti, N.; Berti, C.; Munad, A. *e-Polym.* **2003**.
(10) Pyda, M.; Boller, A.; Grebowicz, J.; Chuah, H.; Lebedev, B. V.; Wunderlich, B. *J. Polym. Sci., Part B: Polym. Phys.* **1998**, *36*, 2499–2511.
(11) Pyda, M.; Wunderlich, B. *J. Polym. Sci., Part B: Polym. Phys.* **2000**, *38*, 622–631.
(12) Wunderlich, B. *Macromolecular Physics*; Academic Press: New York, 1973; Vol. *2*.
(13) Cho, J. W.; Woo, K. S. *J. Polym. Sci., Part B* **2001**, *39*, 1920–1927.
(14) Luo, W.; Liao, Z.; Yan, J.; Li, Y.; Chen, X.; Mai, K.; Zhang, M. *Macromolecules* **2009**, *41*, 7513–7518.
(15) Schönhals, A.; Kremer, F. *Broad Band Dielectric Spectroscopy*: Springer: Berlin, 2002.
(16) Coburn, J. C.; Boyd, R. H. *Macromolecules* **1986**, *19*, 2238.
(17) Ezquerra, T. A.; Balta-Calleja, F. J.; Zachmann, H. G. *Polymer* **1994**, *35*, 2600–6.
(18) Alvarez, C.; Sics, I.; Nogales, A.; Denchev, Z.; Funari, S. S.; Ezquerra, T. A. *Polymer* **2004**, *45*, 3953–3959.
(19) Williams, G. *Adv. Polym. Sci.* **1975**, *33*, 59.
(20) Soccio, M.; Nogales, A.; Lotti, N.; Munari, A.; Ezquerra, T. A. *Polymer* **2007**, *48*, 4742–4750.
(21) Soccio, M.; Nogales, A.; Lotti, N.; Munari, A.; Ezquerra, T. A. *Phys. Rev. Lett.* **2007**, *98*, 037801.
(22) Sanz, A.; Nogales, A.; Ezquerra, T. A.; Lotti, N.; Munari, A.; Funari, S. S. *Polymer* **2006**, *47*, 1281–1290.
(23) Bras, A. R.; Malik, P.; Dionisio, M.; Mano, J. F. *Macromolecules* **2008**, *41*, 6419–6430.
(24) Nogales, A.; Ezquerra, T. A.; Garcia, J. M.; Balta-Calleja, F. J. *J. Polym. Sci., Part B: Polym. Phys.* **1999**, *37*, 37–49.
(25) Cheng, S. Z. D.; Cao, M. Y.; Wunderlich, B. *Macromolecules* **1986**, *19*, 1868–76.
(26) Pyda, M.; Nowak-Pyda, E.; Mays, J.; Wunderlich, B. *J. Polym. Sci., Part B: Polym. Phys.* **2004**, *42*, 4401–4411.
(27) Huo, P.; Cebe, P. *Macromolecules* **1992**, *25*, 902–9.
(28) Dobbertin, J.; Hensel, A.; Schick, C. *J. Therm. Anal.* **1996**, *47*, 1027–1040.
(29) Pyda, M.; Nowak-Pyda, E.; Heeg, J.; Huth, H.; Minakov, A. A.; Di Lorenzo, M. L.; Schick, C.; Wunderlich, B. *J. Polym. Sci., Part B: Polym. Phys.* **2006**, *44*, 1364–1377.
(30) Laredo, E.; Grimau, M.; Muller, A.; Bello, A.; Suarez, N. In *Meeting of the Division of High Polymer Physics of the American-Physical-Society*; John Wiley & Sons Inc.: St. Louis, MO, 1996; pp 2863−2879.
(31) Xu, H.; Cebe, P. *Polymer* **2005**, *46*, 8734–8744.
(32) Nogales, A.; Ezquerra, T. A.; Batallan, F.; Frick, B.; Lopez-Cabarcos, E.; Balta-Calleja, F. J. *Macromolecules* **1999**, *32*, 2301–2308.
(33) Nogales, A.; Ezquerra, T. A.; Denchev, Z.; Sics, I.; Calleja, F. J. B.; Hsiao, B. S. *J. Chem. Phys.* **2001**, *115*, 3804–3813.
(34) Soccio, M.; Lotti, N.; Finelli, L.; Gazzano, M.; Munari, A. *J. Polym. Sci., Part B: Polym. Phys.* **2008**, *46*, 170–181.
(35) Soccio, M.; Lotti, N.; Finelli, L.; Munari, A. *J. Polym. Sci., Part B: Polym. Phys.* **2008**, *46*, 818–830.
(36) Rueda, D. R.; Garcia-Gutierrez, M. C.; Nogales, A.; Capitan, M. J.; Ezquerra, T. A.; Labrador, A.; Fraga, E.; Beltran, D.; Juanhuix, J.; Herranz, J. F.; Bordas, J. *Rev. Sci. Instrum.* **2006**, *77*, 5.
(37) Ezquerra, T. A.; Sics, I.; Nogales, A.; Denchev, Z.; Balta-Calleja, F. J. *Europhys. Lett.* **2002**, *59*, 417–422.
(38) Sics, I.; Nogales, A.; Ezquerra, T. A.; Denchev, Z.; Balta-Calleja, F. J.; Meyer, A.; Dohrmann, R. *Rev. Sci. Instrum.* **2000**, *71*, 1733–1736.
(39) Havriliak, S.; Negami, S. *Polymer* **1967**, *8*, 161.
(40) Nogales, A.; Denchev, Z.; Sics, I.; Ezquerra, T. A. *Macromolecules* **2000**, *33*, 9367–9375.
(41) Kramarenko, V. Y.; Ezquerra, T. A.; Sics, I.; Balta-Calleja, F. J.; Privalko, V. P. *J. Chem. Phys.* **2000**, *113*, 447–452.
(42) Nogales, A.; Sanz, A.; Sics, I.; García-Gutierrez, M. C.; Ezquerra, T. A. *Lectures Notes Physics*; Springer-Verlag: Berlin, 2007.
(43) Sics, I.; Ezquerra, T. A.; Nogales, A.; Denchev, Z.; Alvarez, C.; Funari, S. S. *Polymer* **2003**, *44*, 1045–1049.
(44) Verma, R.; Marand, H.; Hsiao, B. *Macromolecules* **1996**, *29*, 7767–7775.
(45) Zachmann, H. G.; Wutz, C. *Crystallization of Polymers*; Kluwer Academic Publisher: Dordrecht, 1993.
(46) Lee, B.; Shin, T. J.; Lee, S. W.; Yoon, J.; Kim, J.; Ree, M. *Macromolecules* **2004**, *37*, 4174–4184.
(47) Schonhals, A.; Schlosser, E. *Colloid Polym. Sci.* **1989**, *267*, 125–132.
(48) Schlosser, E.; Schonhals, A. *Colloid Polym. Sci.* **1989**, *267*, 963–969.